Minimum Detectable Activity for Tomographic Gamma Scanning System – 15648

Ram Venkataraman *, Susan Smith* , John Kirkpatrick *, Stephen Croft **

* Canberra Industries (AREVA BDNM), 800 Research Parkway, Meriden, CT 06450, USA
** Oak Ridge National Laboratory, One Bethel Valley Road, Oak Ridge, TN 37831-6166, USA

ABSTRACT

For any radiation measurement system, it is useful to explore and establish the detection limits and a minimum detectable activity (MDA) for the radionuclides of interest, even if the system is to be used at far higher values. The MDA serves as an important figure of merit, and often a system is optimized and configured so that it can meet the MDA requirements of a measurement campaign. The non-destructive assay (NDA) systems based on gamma ray analysis are no exception and well established conventions, such the Currie method, exist for estimating the detection limits and the MDA. However, the Tomographic Gamma Scanning (TGS) technique poses some challenges for the estimation of detection limits and MDAs. The TGS combines high resolution gamma ray spectrometry (HRGS) with low spatial resolution image reconstruction techniques. In non-imaging gamma ray based NDA techniques measured counts in a full energy peak can be used to estimate the activity of a radionuclide, independently of other counting trials. However, in the case of the TGS each "view" is a full spectral grab (each a counting trial), and each scan consists of 150 spectral grabs in the transmission and emission scans per vertical layer of the item. The set of views in a complete scan are then used to solve for the radionuclide activities on a voxel by voxel basis, over 16 layers of a 10x10 voxel grid. Thus, the raw count data are not independent trials any more, but rather constitute input to a matrix solution for the emission image values at the various locations inside the item volume used in the reconstruction. So, the validity of the methods used to estimate MDA for an imaging technique such as TGS warrant a close scrutiny, because the pair-counting concept of Currie is not directly applicable. One can also raise questions as to whether the TGS, along with other image reconstruction techniques which heavily intertwine data, is a suitable method if one expects to measure samples whose activities are at or just above MDA levels. The paper examines methods used to estimate MDAs for a TGS system, and explores possible solutions that can be rigorously defended.

INTRODUCTION

TGS systems have been commercially employed in assaying radioactive waste generated by facilities handling special nuclear materials (SNM) as well as nuclear power plants[1,2,3]. The methodology has been in common use sufficiently to warrant the release of an ASTM (American Society for Testing and Methods) standard to streamline its application[4]. One of the characteristics of the NDA methods that have been used traditionally in waste assay applications is the MDA. The MDA is often one of the specifications that is used by end-users when selecting a technique for waste assay. Since the TGS method quantifies nuclide activities using imaging techniques, care must be taken while evaluating the measurement needs, and in comparing the characteristic of various instruments to the TGS. Image reconstruction, more specifically attenuation corrected

mass (or activity) image reconstruction, typically requires high quality data, in excess of what would usually be thought of as marginal statistical quality.

Tomographic data is obtained by scanning a cylindrical container with radioactive waste in three degrees of freedom; vertical, rotation, and translation. The item is continuously rotated and translated across the field of view of a collimated High Purity Germanium (HPGe) detector and a transmission source while a large number of full spectral grabs or view data are acquired. These view data correspond to the different projections of the container matrix and its contents, and are used to solve for transmission and emission maps of the item on a voxel by voxel basis. Image reconstruction algorithms are then applied to the attenuation-corrected emission maps across the entire drum to determine the radionuclide content. The analysis is done for each gamma line of interest using ROI peak area analysis for reasons of speed and statistical validity and robustness, given that each spectral grab is typically of very short duration (0.75 seconds).

As image reconstruction algorithms are used in the TGS technique, there is the question as to how accurate or representative is the industry-standard Currie Formalism for the MDA calculation. This paper is investigates the application of the Currie MDA to the TGS technique through analytical and experimental methods.

MDA METHODS FOR TGS BASED ON CURRIE FORMALISM

Following the Currie formalism[5], the Critical Limit (L_C), and the Detection Limit (L_D) are defined for the TGS analysis on the basis of the counts in the continuum Regions of Interest (ROI) to the left and right of a peak ROI, accumulated over the emission scan of the entire item. Besides the Critical Limit and the Detection Limit, another useful quantity called the “Less than limit” or L_t is defined for the TGS.

The extent (number of channels) of the continuum (or background) ROIs to the left and right of a peak ROI may not be equal as they are user-defined and therefore are weighted to determine the peak continuum. The equations below give the counts in the background ROIs, and the uncertainty in the counts.

$$B = W_1 B_1 + W_2 B_2$$
$$\sigma_B^2 = W_1^2 B_1 + W_2^2 B_2 = G + W_1^2 B_1 + W_2^2 B_2 \qquad \text{- (1)}$$

B_1 and B_2 correspond to the left and right background ROIs, respectively, and W_1 and W_2 are the corresponding weighting factors. Since Poisson behavior is adopted, mean is equal to the variance of the counts.

The net signal S and its uncertainty are given in equation (2) below.

$$S = G - B$$
$$\sigma_S^2 = \sigma_G^2 + \sigma_B^2 \qquad \text{- (2)}$$

In equation (2), G is the gross counts in the peak ROI, and B is the background counts as defined in equation (1). At the Critical Limit, the signal is indistinguishable from the background. In other words, the true signal goes to zero. The uncertainty in the null signal σ_0 is calculated as follows.

$$\sigma_o^2 = B + \sigma_B^2 \quad \text{- (3)}$$

The Critical Limit is $k\sigma_0$, where k is the one-sided confidence factor for the Gaussian distribution (large number, Poisson limit). Equation (4) gives the Critical Limit as implemented for the TGS in the NDA2000 software.

$$L_c = k\sqrt{W_1 B_1 + W_2 B_2 + W_1^2 B_1 + W_2^2 B_2} \quad \text{- (4)}$$

The *detection limit* L_D which represents the minimum signal that can be detected above background at a given confidence level is defined for the TGS following the Currie formalism.

$$L_D = k^2 + 2L_c \quad \text{- (5)}$$

Once the detection limit is defined, the MDA for a given nuclide is determined by factoring in the efficiency and the gamma ray yield. In equation (6) below, ε is the efficiency and t is the total counting time for the emission scan.

$$MDA' = \frac{L_D}{\varepsilon' \cdot t} \quad \text{- (6)}$$

The efficiency factor deserves a closer examination since it is intertwined with the image reconstruction used by the TGS to solve for the radionuclide concentration on a voxel-by-voxel basis. The un-calibrated response of a TGS measurement, called the "TGS Number" is given in terms of emission image vectors (S_j) summed over all voxels (j). The emission image in a given voxel is the raw count rate from that voxel, corrected for the geometrical efficiency (solid angle subtended by that voxel at the detector), the energy dependent attenuation correction for that voxel (from the transmission map), and the rate loss correction based on a pulser or a rate loss source. The TGS Number, calculated for a given gamma line from a nuclide, is thus proportional to the line activity of the nuclide.

$$TGSNumber(E) = norm \cdot \sum_j S_j \quad \text{- (7)}$$

The "norm" factor in equation (7) corrects for any differences between the total counts from the reconstructed image and the sum of counts registered over all views in the emission scan.

The TGS Number is calibrated by measuring the response of a radionuclide source of known activity. Determining the calibration factor at a given emission energy is expressed (e.g.) as follows;

$$CalibFactor(E) = \frac{gammas/sec}{TGSNumber(E)} \quad \text{- (8)}$$

With all the necessary quantities and terminology defined in equations (7) and (8), the efficiency function for a uniform distribution of activities over all voxels can now be written as follows.

$$eff(uniform) = \frac{\Sigma_{ij} F_{ij}}{CalibFactor(E) \cdot N_{views} \cdot N_{voxels}} \quad \text{- (9)}$$

F_{ij} is an element of the attenuation corrected efficiency matrix corresponding to the i-th view and j-th voxel. Since the elements of the F matrix are summed up, it is necessary to divide by N_{voxels} and N_{views} in order to compute the average efficiency. Dimensionally, the product of the TGS Number (which is the same as the emission image S_j summed over all voxels) ΣF_{ij} is the same as the count rate in the view data. Thus efficiency has the dimensions of counts/sec per gammas/sec, which is the familiar definition of peak efficiency in gamma spectrometry. The MDA results reported in this paper are estimated based on the assumption of uniform distribution of radioactivity in the item matrix. Other choices are possible and could be guided by acceptable process knowledge. The choice of a uniform distribution seems reasonable when no other guidance is available (e.g. the image is uninformative) and since typically one is concerned with a consignment average over a number of drums.

MEASUREMENT OF TGS MDA

The MDAs were estimated experimentally using Canberra's CAN-TGS system (Figure 1). The Can-TGS system is a modular design consisting of a miniature mechanism (Lift, Traverse and Turntable), a transmission source with a shutter assembly, and a HPGe detector shield / collimator assembly. All three assemblies are secured to a mechanism base-plate which is approximately 91.4 cm wide x 121.9 cm deep. The mechanism control electronics enclosure is also mounted to this base-plate. The mechanism lift provides approximately 34.3 cm of linear vertical motion and the traverse provides approximately 29.2 cm of horizontal motion. Both drives are operated via stepper motors. The rotation is controlled via a servo direct drive motor and servo controller. The servo provides feedback to smoothly control the rotation motion. The rotator is 31.8 cm diameter and has machined centering guides for precision locating the many sample sizes the Can-TGS is able to accommodate. The maximum lift capacity of the mechanism is approximately 113.4 kg. The mechanism control system is a Programmable Logic Controller (PLC) based controller. The PLC controller is based on the same controller architecture as Canberra's standard TGS System. A touch screen control panel is provided with the system to allow local or remote control of the mechanism.

The Canberra Can-TGS system utilizes an HPGe detector of the Broad Energy type, model BE5030, housed inside a cylindrical lead shield with a thickness of 5.08 cm. The HPGe detector is collimated by a tungsten collimator and aperture arrangement. The collimator can be configured with apertures of different sizes, depending on the container geometry and the desired spatial resolution of the image. In this work, a diamond shaped collimator, typical of TGS operation, with an aperture of 25.4 mm was used with the detector recessed to 100 mm. The Can-TGS system uses a Eu-152 transmission source with a nominal activity of 15 milli-Curies ($5.55*10^8$ Bq).

Fig. 1. Canberra's Can-TGS System for Small Containers

The MDA measurements were performed for a 5 gallon steel pail filled with walnut shells and a matrix density of 0.67 $g.cm^{-3}$ without radioactive sources. The pail has a diameter of 11.875" (302mm) and a height of 13.35" (339mm). Using the 1" (25.4mm) truncated diamond collimator geometry, the container was divided into a 10x10 voxel matrix per layer and 16 segments. One hundred fifty (150) views (data grabs) were acquired per segment. In total, 75 replicate assays were performed, each with a total emission counting time of 1800 seconds.

Table 1 below presents the average TGS MDA for selected nuclides based on the results of the TGS MDAs measurements for the 5 gallon pail geometry. The individual assay MDA values were reported by NDA 2000 using the Currie formalism at the 95% confidence level and the average efficiency of the entire drum.

Table 1. Selected MDAs of the Can-TGS

Nuclide	Gamma ray energy (keV)	MDA (μCi)	MDA (kBq)	MDC (Bq/g)
^{133}Ba	356.01	0.460	17.02	1.34
^{137}Cs	661.67	0.502	18.56	1.46
^{60}Co	1332.50	0.212	7.83	0.62

EXPLORING THE SENSITIVITY LIMITS OF THE TGS

The Critical Limit L_C was established at 95% confidence level for gamma ray peak ROIs from the measurements described previously. Next, assays were performed with a single point source of a given radionuclide (^{133}Ba, ^{137}Cs, ^{60}Co) with progressively diminishing activities. The source was placed at the bottom of the pail as the voxels here would have some of the lowest efficiencies in a TGS measurement Again, the counting time of 1800 seconds corresponded to the emission scan time of the assay. For each source, a total of 20 assay trials were performed. For each assay, the net counts in the peak ROIs of the given nuclide were determined and compared with the critical limit established for the ROI for that nuclide. If the net counts in the peak ROI are greater than L_C, the peak is considered statistically significant. The percentage of trials for which the net counts in the net peak ROI was greater than L_C was computed for each source. The results are given in Table 2.

Table 2. Sensitivity of Can-TGS

Nuclide	Source Strength (μCi)	% trials (Net Peak count > L_C)
^{133}Ba (356 keV)	0.237	35%
	0.48	85%
	0.68	90%
	1.40	100%
^{137}Cs (662 keV)	0.26	75%
	0.55	100%
	0.732	95%
	0.902	100%
^{60}Co (1332 keV)	0.25	85%
	0.50	100%
	0.793	100%
	0.997	100%

The number of assay trials conducted with each source was only 20 and therefore strictly not enough to determine the MDAs to a high level of confidence through experimentation, since a large number of assay trials are needed to map out the tails of the distribution.

Nevertheless, quantitative inferences can be drawn from these results. By assuming that the results of the trials are binomially distributed about some detection probability *p*, Bayes' theorem can be used (along with the assumption of a uniform prior probability distribution) to infer the value of *p* for each source. Given *n* detections (defined by a trial with peak counts in excess of the critical level) out of *m* trials, the expectation value of the detection probability *p* is

$$\langle p \rangle = \frac{n+1}{m+2} \qquad \text{- (10)}$$

The uncertainty in this estimate is given by

$$\sigma(p) = \sqrt{\frac{(n+1)}{(m+2)}\left(\frac{(n+2)}{(m+3)} - \frac{(n+1)}{(m+2)}\right)} \qquad \text{- (11)}$$

The detection probabilities estimated by this method, for each measured source listed in Table 2, are plotted in Figure 2. For each nuclide, the estimated detection probability is shown as a function of activity; the 95% detection probability corresponding to the MDA is indicated with a solid line. The lowest measured activities of ^{133}Ba and ^{137}Cs are below the MDA and estimated to have detection probabilities significantly less than 95% as is expected. For ^{133}Ba at 0.48 μCi, just above the calculated MDA, the estimated detection probability is within two standard deviations of 95%, and so generally consistent with expectation. Similarly, for ^{137}Cs the 0.55 μCi source is just above the calculated MDA, and the estimated detection probability at that activity is consistent with 95%. The lowest measured ^{60}Co activity just exceeds the detection limit for that nuclide and again, the estimated detection probability is consistent, within two sigma, with the expected 95% value.

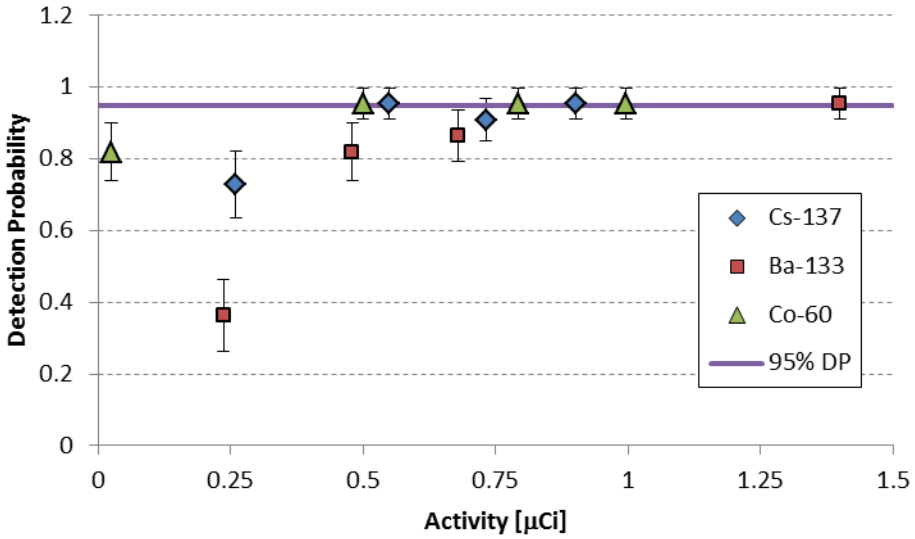

Fig. 2. Estimated detection probabilities by nuclide and activity for Table 2 sources

It is interesting to note that, for example, the estimated detection probability for the 0.48 μCi ^{133}Ba source and the 0.55 μCi ^{60}Co source are just above 80%, close to but slightly less than the observed frequency of 85% from Table 2. A small bias toward moderate values is a feature of this method of Bayesian inference of a binomial probability using a uniform prior: equation (10) will never predict $p = 0$ or 1, even for $n = 0$ or m .However, the observed frequency is always within about one sigma of the estimated probability. Examination of the emission images obtained from the assay of radionuclides of various source strengths, in conjunction with the comparison of net peak ROI counts with the critical limit, were also used to evaluate whether the Currie formalism is a good enough approach to estimate the sensitivity of the TGS method. For example, for net peak ROI counts that are well above the critical limit, one can expect sharp images of the radionuclide distribution. As the source strength decreases, the net peak count approaches the critical limit and the emission image becomes blurred and noisier. This is because poor counting statistics used in image reconstruction result in a solution that is less constrained and the emission image tends to spread out into neighboring voxels. This theory was tested using the TGS measurement results.

In order to use a consistent criterion, the emission image from the assay trial that yielded the closest net peak ROI counts to the average value based on the 20 trials with the given source, was selected for studying the trends. The net peak count obtained in this representative assay trial was compared to the critical limit (L_C) established at the 95% confidence level ("conf."), shown in Table 3. The critical limit had been established by assaying a non-radioactive matrix of density 0.67 g·cm^{-3} (Table 1). The images generated in the corresponding TGS assays are shown in Figures 3a-3d, Figures 4a-4d, and Figures 5a-5d.

Table 3. Comparison of Net Peak ROI Counts vs. Critical Limit (L_C)

Nuclide (γ line)	Source Strength (μCi)	L_C (Counts) (95% conf.)	Net Peak ROI (Counts)
^{133}Ba (356 keV)	0.237	16	10
	0.48	16	27
	0.68	16	33
	1.40	16	83
^{137}Cs (662 keV)	0.26	18	23
	0.55	18	46
	0.732	18	42
	0.902	18	66
^{60}Co (1332 keV)	0.25	8	15
	0.50	8	40
	0.793	8	64
	0.997	8	72

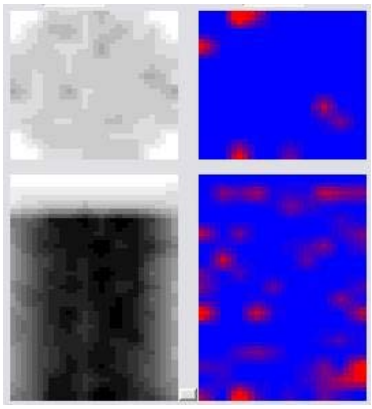

Figure 3a. ^{133}Ba – 0.237 μCi

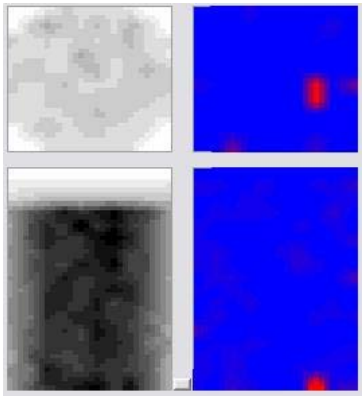

Figure 3b. ^{133}Ba – 0.48 μCi

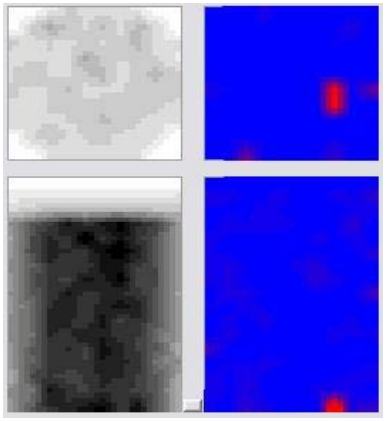

Figure 3c. ^{133}Ba – 0.68 μCi

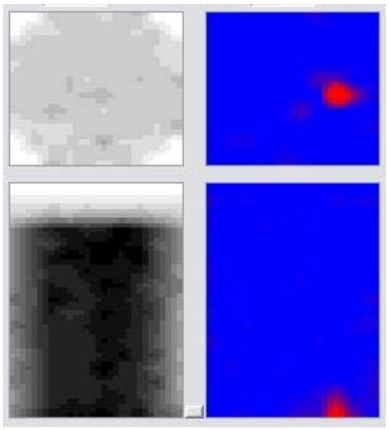

Figure 3d. ^{133}Ba – 1.4 μCi

In Figures 3a-3d, and indeed in other images that are shown in Figures 4a-4d and 5a-5d, the images on the left in gray scale are the transmission images (linear attenuation coefficient map) of the container matrix and the images on the right depict the emission images of radionuclide activity. The images at the top of each figure display the vertical layer of the matrix where the source activity is present. In the current measurement campaign, a single point source of a given radionuclide was located at the bottom of the item. The emission images in Figures 3b, 3c, and 3d reveal that the ^{133}Ba source location is correctly imaged by the Can-TGS. The transmission images in Figures 3a-3d do not show any variation since they are based on the transmission scan data from the same ^{152}Eu transmission source and a uniform matrix. The emission image from the weakest ^{133}Ba source (Figure 3a), whose net peak ROI counts was less than $L_{C,}$ shows that the counts from the nuclide are not statistically significant when compared to the background fluctuation. The emission images in Figures 3b, 3c, and 3d seem to be of the same quality, although there is some evidence of noise in the images shown in Figures 3b and 3c.

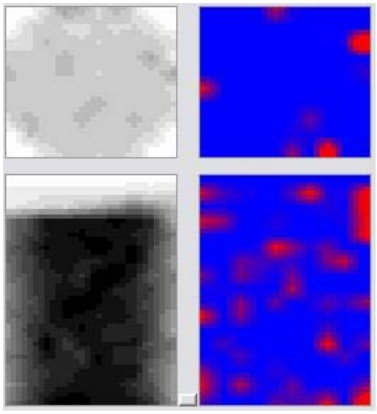

Fig. 4a. ^{137}Cs – 0.26 μCi

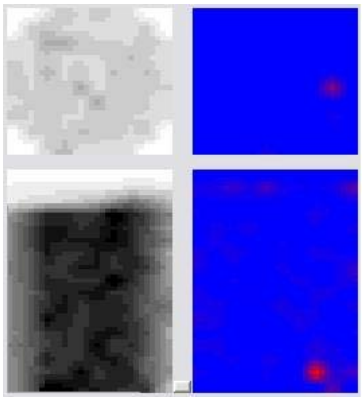

Fig. 4b. ^{137}Cs – 0.55 μCi

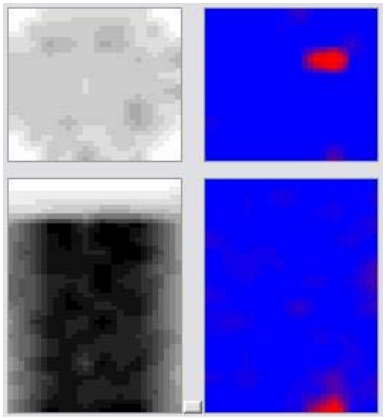

Fig. 4c. ^{137}Cs – 0.732 μCi

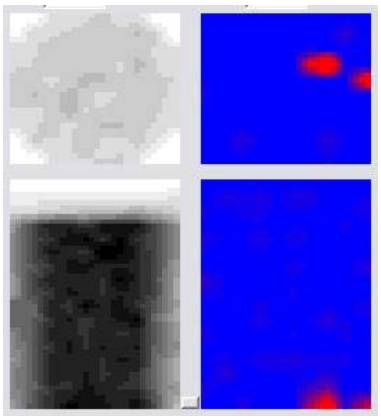

Fig. 4d. ^{137}Cs – 0.902 μCi

The net peak ROI count from the weakest ^{137}Cs source is just above the critical limit. The emission image from the assay of this source (Fig. 4a) is very noisy and shows that the source activity is not statistically significant compared to the background. The emission images of the other three ^{137}Cs sources are not noisy (Figs. 4b, 4c, 4d), and the source activity is at the correct location. In figure 4d, the emission image is sharp, but seems to have been split between two close voxels. Even though the peak ROI count from the 0.902 μCi is well above the critical limit, the precision of the data is still poor, with very few counts registered in each view. This clearly demonstrates how poor counting statistics used in image reconstruction result in a less constrained solution and emission images that spread into neighboring voxels.

Figures 5a-5d show the emission images from the assay of single ^{60}Co source. The source strengths and the critical limit are given in Table 3.

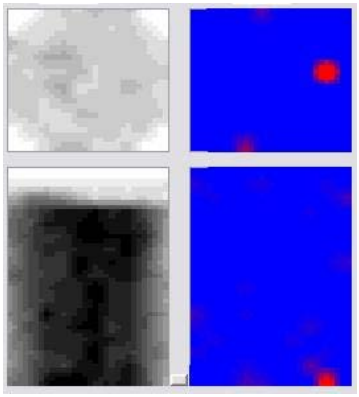

Fig. 5a. ^{60}Co – 0.25 μCi

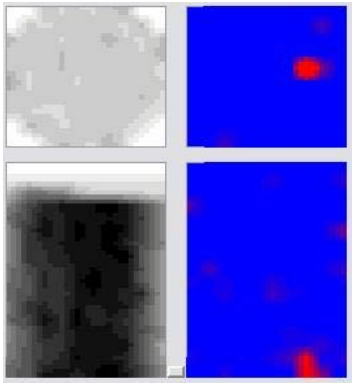

Fig. 5b. ^{60}Co – 0.50 μCi

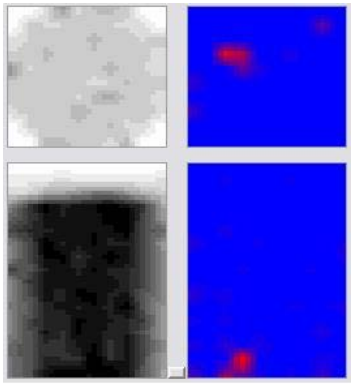

Fig. 5c. ^{60}Co – 0.793 μCi

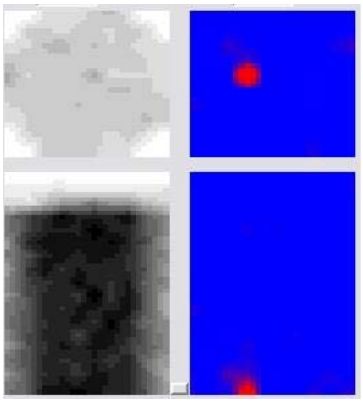

Fig. 5d. ^{60}Co – 0.997 μCi

The emission image for the weakest ^{60}Co is not noisy. The net peak ROI count in the 1332 keV peak is greater than the critical limit. The activity level of the source (0.25 μCi) is just above the estimated MDA value (detection limit) given in Table 1 for ^{60}Co. The emission images of the three higher activity ^{60}Co sources appear to be sharp. It is interesting to note that the emission images in Figures 5c (0.793 μCi) and 5d (0.997 μCi) are at a different location within the container matrix compared to the images in Figures 5a and 5b. This is consistent with the actual location of the source within the container. While the goal was to maintain the same location of the source for all assays, the 0.793 μCi and the 0.997 μCi sources were inadvertently placed at a different location. The assays with "incorrect" source locations turned out to be advantageous in that this was yet another test of the imaging performance of the Can-TGS. Due to limitations of space, only a few of the images that were generated in this work could be included in the paper. A more exhaustive set of images are available from the lead author through private communication.

CONCLUSIONS

Following the Currie formalism, the critical limit and the MDA were established at the 95% confidence level for gamma ray peak ROIs corresponding to radionuclides ^{133}Ba, ^{137}Cs, and ^{60}Co by assaying a non-radioactive item matrix using Canberra's Can-TGS. The item was a 5 gallon pail with a representative matrix of density 0.67 g.cm^{-3}. A 1" (25.4 mm) truncated-diamond shaped tungsten collimator was used in the assays. The sensitivity limits of the Can-TGS were explored by assaying sources with progressively decreasing strengths and comparing the net peak ROI counts at the energy of interest to the critical limit. The quality of the emission images obtained from the assays correlated well with the net peak ROI counts versus the critical limit comparison. This boosts the confidence that the Currie method can indeed be applied to define and establish the MDA limits for the TGS method in both a familiar way and one which is defensible and fit for purpose.

REFERENCES

1. R. J. Estep, T. H. Prettyman, G. A. Sheppard, *Tomographic gamma scanning to assay heterogeneous radioactive waste*, Nuclear Science and Engineering; Nov. 1994; vol.118, no.3, p.145-52.
2. R. Venkataraman,, M. Villani, S. Croft, P. McClay, R. McElroy, S. Kane, W. Mueller, R. Estep, *An integrated tomographic tamma scanning system for non-destructive assay of radioactive waste*, Nucl. Inst. Meth. in Phys. Res. A 579 (2007), 375-379.
3. S. Croft, D.S. Bracken, S.C. Kane, R. Venkataraman and R. J. Estep, *Bibliography of Tomographic Gamma Scanning Methods Applied to Waste Assay and Nuclear Fuel Measurements*, Proceedings of the 47th Annual Meeting of the INMM (Institute of Nuclear Materials Management), 16-20 July 2006, Nashville, Tennessee, USA.
4. P.J. LeBlanc, J. Lagana, J. Kirkpatrick, D. Nakazawa, S. Kane Smith, R.Venkataraman, M.Villani, and B. M. Young, *Characterization of Canberra's tomographic gamma-ray can scanner ("Can-TGS")*, Proceedings of Waste Management 2013 Conference, February 24 – 28, 2013, Phoenix, Arizona, USA
5. *Standard Test Method for Nondestructive Assay of Radioactive Material by tomographic gamma scanning*, ASTM Standard C1718-10, ASTM International.
6. Lloyd A. Currie, *Limits for qualitative detection and quantitative determination: application to Radiochemistry*, Anal. Chem. 40, 586-593 (1968).

ACKNOWLEDGEMENTS

One of the authors (Stephen Croft) acknowledges support from U.S. DOE NNSA NA-22 Uncertainty Quantification Project.